Plasmonics (2017) 12:1709–1715
DOI 10.1007/s11468-016-0437-5

CrossMark

Photocurrent Enhancement in Si-Ge Photodetectors by Utilizing Surface Plasmons

Mehdi Afshari Bavil [1] · Zhi Liu [1] · Wenzhou Wu [1] · Chuanbo Li [1] · Buwen Cheng [1]

Received: 8 August 2016 / Accepted: 9 November 2016 / Published online: 19 November 2016
© Springer Science+Business Media New York 2016

Abstract A circular slit-groove surface plasmon polaritons (SPPs) launcher surrounding a photodetector is employed theoretically to enhance the photocurrent of atypical Si-Ge photodetectors. The slit and grooves are designed such that the SPPs are focused at the center of the absorption layer of the photodetector to result in additional electric current. Fabry–Perot resonance condition accurately calculates the period of the groove, slit-groove distance, photodetector radius, and slit-photodetector distance. The manipulation leads to constructive interference between the incident light impinging from the top and the SPPs propagating toward the photodetector. Simulation result shows that photocurrent increases by approximately 13-fold when the SPPs are introduced.

Keywords Surface plasmons · Fabry-Perot resonance · Photodetectors · Silicon

Introduction

Photodetectors, which convert optical signals into electrical signals, are highly important in optical communication [1]. Detectors with ability of detecting extremely low-intensity light signals, such as P-N junction detectors [2–4], metal–semiconductor–metal detectors [5, 6], avalanche photodetectors [7–9], and separate absorption, charge, and multiplication structures [10–12], have been developed. Si has been recognized as an excellent photodetector material compared with III–V-based devices because of its lower multiplication noise [13, 14]. However, another material should be introduced to adjust the absorption at telecommunication wavelengths. Ge is a feasible candidate because of its compatibility with complementary metal oxide semiconductor (CMOS) despite the 4% mismatch in the lattice constants between Ge and Si [15, 16].

Surface plasmon polaritons (SPPs) are electromagnetic waves that propagate at the interface between a metal and a dielectric layer beyond the diffraction limit [17, 18]. Nanoplasmonics exploits surface plasmons that can control and manipulate optical signals to provide a platform for developing and optimizing various nanophotonic components, especially photodetectors [19–22]. Potential geometries to excite SPPs are direct-coupling configurations, such as sub-wavelength nanohole arrays and nanoslits drilled on the metal contact of the light-radiating surface capable of extraordinary transmission [23–25]. However, the high reflectivity of the metallic layer on the radiation side and very low light transmission through the holes and slits remarkably limit these geometries, resulting in very low photodetector sensitivity. Side-coupling of SPPs via grooves [26], patches [27], and circular grating [28, 29], which the SPPs can control and unidirectionally propagate, is another approach to efficiently excite SPPs.

In this paper, we propose, design, and demonstrate a novel plasmonic-based photodetector with operating wavelength of 1550 nm to enhance the photocurrent. Our proposed structure has a circular configuration and includes sub-wavelength slit and grooves in a metallic layer surrounding a Si-Ge photodetector at the center. SPPs can be steered to predominantly propagate toward the center by tailoring the distance between the slit and grooves and the separation between the core and slit. The most important feature of this structure is that the top electrode ring can be as narrow as possible to avoid light reflection. Geometrical parameters are obtained theoretically

✉ Chuanbo Li
cbli@semi.ac.cn

[1] State Key Laboratory on Integrated Optoelectronics, Institute of Semiconductors, Chinese Academy of Sciences, Beijing 100083, China

to provide the maximum absorption at our working wavelength. Commercial package (Lumerical simulation) of the finite difference time domain simulation is used to study the plasmonic photodetector.

Theoretical Approach and Discussion

The 3D view, top view, and cross-section along a perpendicular plane of the proposed structure is shown in Fig. 1. The central part shows the configuration of the Ge-Si photodetector. The layer properties from the bottom are as follows: bottom contact; 500 nm Si layer with N^+ doping of 1×10^{19} cm^{-3}; 500 nm Si multiplication layer with N doping of 4.5×10^{16} cm^{-3}; 100 nm Si charge layer with P doping of 1.5×10^{17} cm^{-3}, 100 nm Si interface layer with P doping of 1×10^{15} cm^{-3}; 1000 nm Ge absorption layer with P doping of 1×10^{15} cm^{-3}; 380 nm Ge layer with P^+ doping of 4×10^{19} cm^{-3} and top contact. The top and bottom contact layers are removed for simplicity in 3D view. In practical configuration, slit-grooves are not complete rings as shown in top view Fig. 2b to assure the function of top electrode. In spite of this incompleteness, simulation result shows the variation is unremarkable.

The narrow layers between the multiplication and absorption layers are doped to adjust the electric field between these layers. The high electric field in the multiplication layer ensures high gain, whereas the low electric field in the absorption layer ensures carrier drift without multiplication. The narrow Si interface layer between the charge and absorption layer may attract extra charge, reducing the electric field in the multiplication region.

A narrow dielectric (SiO_2) layer is considered to prevent the creation of a Schottky barrier between the metallic and semiconductor layers. Consequently, the metallic layer does not affect the electronic properties of the detector. Thus, the proposed structure can be replaced by a bare Si-Ge photodetector to study the band profile and electrostatic field (Fig. 2). Figure 2a shows the electrostatic field at breakdown voltage, and Fig. 2b shows the band profile at zero voltage. The electronic properties of the photodetector can be tailored by changing the doping and thickness of the layers. This process has been widely investigated by researchers and semiconductor band gap engineers [30, 31].

The central region (photodetector), which will be called the core, is surrounded by a gold film, including a sub-wavelength slit-groove SPPs launcher. The film thickness should be larger or equal to the thicknesses of the charge and insulator layers to ensure high coupling of SPPs with illuminated light on the absorption layer. The dielectric permittivity values of gold

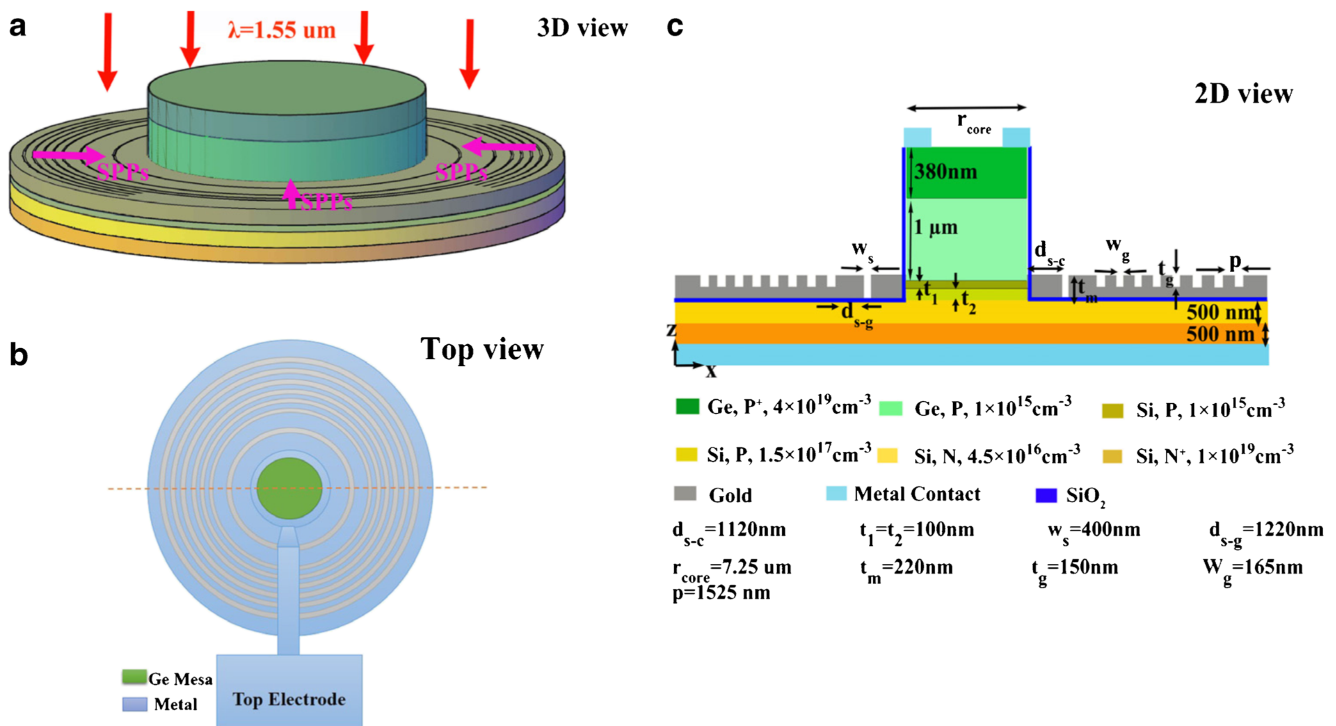

Fig. 1 Schematic of the proposed structure. **a** 3D, **b** top view, and **c** cross-section along the perpendicular plane that is shown in top view in orange color. Layers are presented in different colors to represent the doping and materials. The central part is a conventional Si-Ge photodetector. The layers from the bottom are as follows: bottom contact, Si layer, Si multiplication, Ge charge, Ge interface, Ge absorption, Ge cap layer, and top contact. The narrow SiO_2 layer functions as an insulator to prevent charge transportation. Geometrical parameters and doping of the various layers are presented in the legend

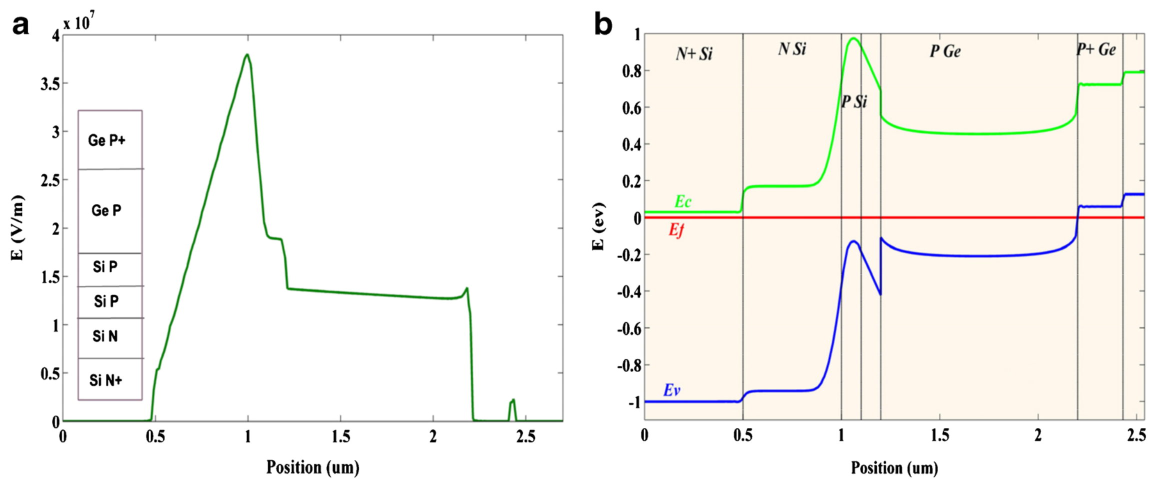

Fig. 2. **a** Electrostatic field of the proposed structure at breakdown voltage. **b** Band structure profile of the proposed structure

are from [32]. SPPs propagating toward the core will excite excitons (electron-hole pairs) in the absorption layer, resulting in an additional electric current. The fabrication processes can be summarized as follows. Different Ge and Si layers can be grown using molecular beam epitaxy. Photolithography can be used to keep the central region. The narrow dielectric (SiO_2) and metallic layers can be deposited. Slits and grooves can be created by milling. Finally, p- and n-type metallization can be created by thermal evaporation.

The generation rate, which is a measurement of absorption, should be considered to show the effect of various geometries on photodetector operation, especially photocurrent. The generation rate is the integration of g (the number of absorbed photons per unit volume) over the simulation spectrum where g is given by:

$$g = \frac{P_{\mathrm{abs}}}{\hbar\omega} = \frac{-0.5|E|^2 \mathrm{imag}(\varepsilon)}{\hbar} \quad (1)$$

where E is electric field (as function of space), $\hbar$ is Dirac's constant, and is dielectric function of materials. However, another parameter should be introduced to gain more insight, because the generation rate is a function of space. *Jsc* is the short-circuit current density (unit: A/m^2), which is equal to the amount of photocurrent generated in the detector. In an ideal case, assuming that all absorbed photons generate electron-hole pairs, the photo-generation current can be obtained: $I = eg$ where e is electron charge, By using the *charge* solver, short-circuit current density can be obtained. This parameter is more appropriate than the generation rate to illustrate how the photocurrent changes when different configurations are considered.

Our structure is of single wavelength, so the geometrical parameters should be optimized to obtain high photocurrent at this wavelength. When the light passes through different media, each medium works as Fabry–Perot (F–P) cavity, and the transmission profile will show minima that can be obtained via F–P resonance conditions [33]. These criteria are rarely considered in the design of photodetectors. Meanwhile, the breakdown voltage and photocurrent vary dramatically when the absorption and multiplication thicknesses change the electrostatic profile based on the principle of semiconductor and charge continuity. Thus, the device should be designed carefully. Only the thickness of the cap layer can be tailored to avoid the deep transmission points.

Figure 3 illustrates how *Jsc* changes by varying the thickness of the absorption and cap layers, given that these layers are Ge. The deep points in the *Jsc* profile correspond to the theoretical predictions. The profile has

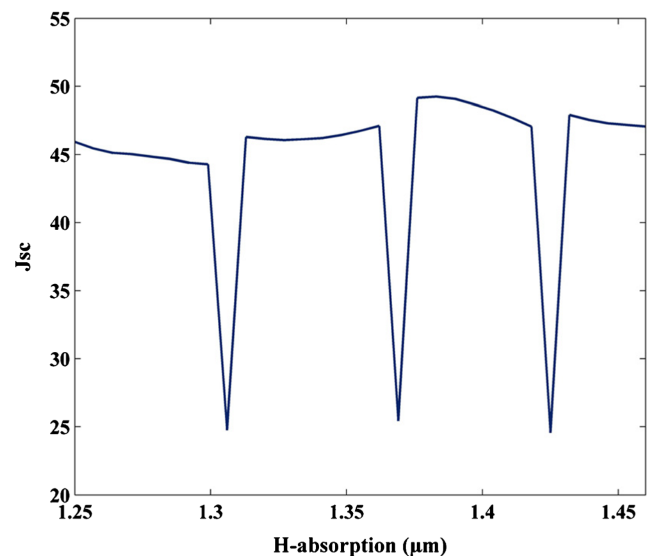

Fig. 3. Variation in *Jsc* versus cap + absorption layer thickness. A periodic behavior with periodicity of 57 nm is observed, which is consistent with the theoretical result

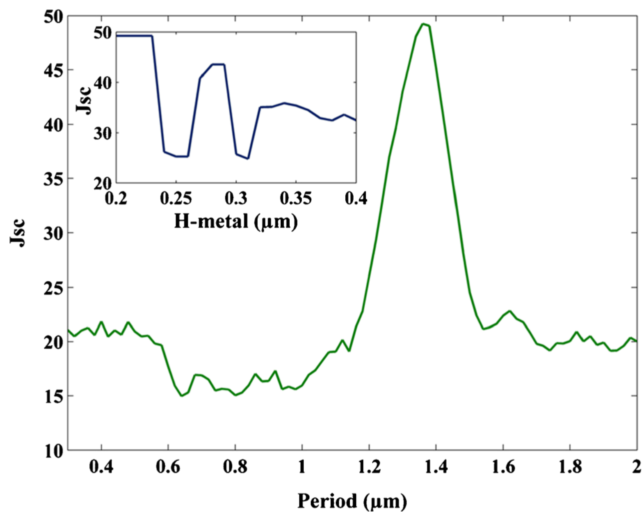

Fig. 4 Variation in *Jsc* versus the period of grooves is in good agreement with theoretical predictions. The inset shows the variation in *Jsc* versus the metallic layer thickness

periodic behavior with periodicity of approximately 57 nm, which is in good agreement with the F–P resonance condition, as follows:

$$h_{\text{cap}} = \frac{m\lambda}{2n\pi} \quad (2)$$

where m is the integer number and represents the resonance order, λ is the electromagnetic wavelength, and n is the refractive index of Ge. According to the result for the first order of resonance, the thickness of 380 nm for the cap layer, which has been optimized through electronics calculations, is a proper thickness. This criterion can be applied to the photodetector radius accordingly. For this case, *Jsc* is also periodic. However, we skipped this calculation for brevity, because the higher resonance orders will be excited and result in periodicity of less than 60 nm. A radius of 7.25 μm is the proper value to achieve higher *Jsc*.

SPPs should be excited at a distance away from the absorption layer and controlled to propagate unidirectionally toward the desired direction. For our working wavelength, the distances of the slit-groove and slit-core should be tailored carefully to guarantee SPPs traveling toward the absorption layer and interference constructively. The design of this device is hinged on two principles [23]. First, the reflection of SPPs by periodic grooves present maxima that can be obtained from their spectral location when the dispersion relation of SPPs satisfies the following expression:

$$kP = m\pi. \quad (3)$$

where P is the period of the array, k denotes the in-plane plasmon wave vector, and m is the band index. Remarkably, their spectral locations do not depend on the groove geometry (width and depth) and the number of grooves, contrary to the reflectance maxima. Second, the phase picked up by the SPP during reflection is only $m\pi$, precisely at the condition given by Eq. (3). We consider an array of ten grooves (later we confirm our choice) with a period $P = 1525$ nm obtained from Eq. (3) with $m = 1$. The depth of the grooves is set to $w = 150$ nm, whereas the widths of the grooves and slit are 165 and 400 nm, respectively. Figure 4 shows the variation in Jsc for different periods obtained from simulation, which shows good agreement with Eq. (3). The variation in Jsc versus metal thickness is shown in the inset of Fig. 4. The thickness of the metallic layer can affect the value of Jsc. The thickness of 220 nm, which is also the sum of the charge and interface layer thicknesses, exhibits higher *Jsc*.

Thus, the configuration for the efficient unidirectional launching of SPPs can be obtained. SPPs propagating from

Fig. 5 Variation in *Jsc* versus interspace distance between the slit and the **a** first groove and **b** core region. The peaks correspond with Eq. (3). The higher resonance orders are also excited. We focus on the first orders for our structures

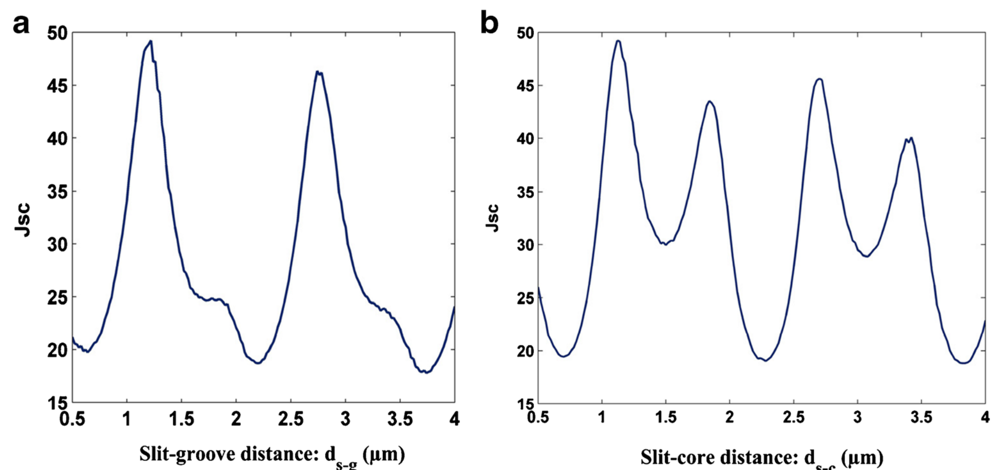

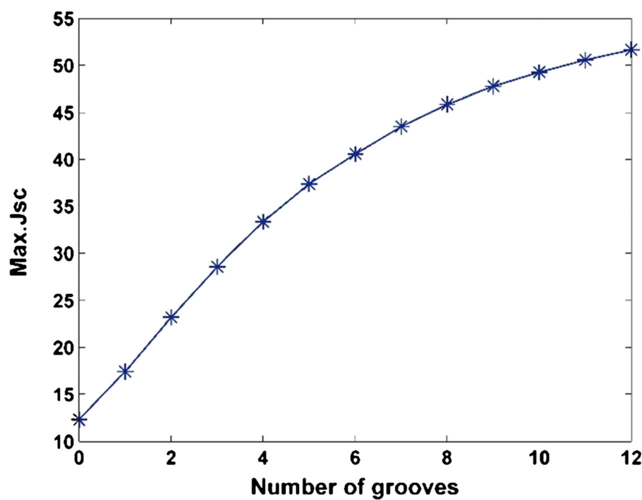

Fig. 6 Variation in the maximum *Jsc* with groove number. The enhancement rate becomes lower for cases with more than ten grooves

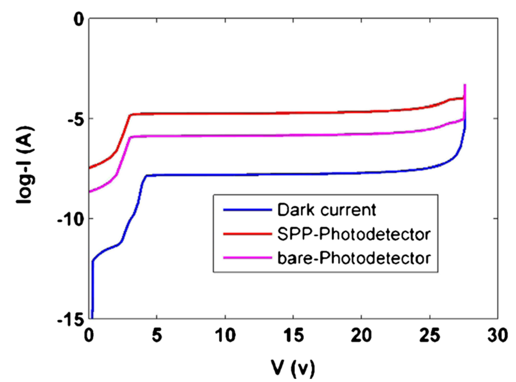

Fig. 8 I–V profile of the proposed structure, dark current, and bare Si-Ge photodetector

the slit toward grooves will be mainly backscattered. The separation, d, between the slit and the first groove of the array (defined center to center) is another important parameter that should be calculated precisely to tune the interference of the reflected SPP with the one leaving the slit toward the groove.

The total phase difference, φ, between the two interfering SPPs will be the phase selected during reflection plus the one associated with their different path lengths along the metal [23], as follows:

$$\varphi = 2kd_{s-g} + m\pi \tag{4}$$

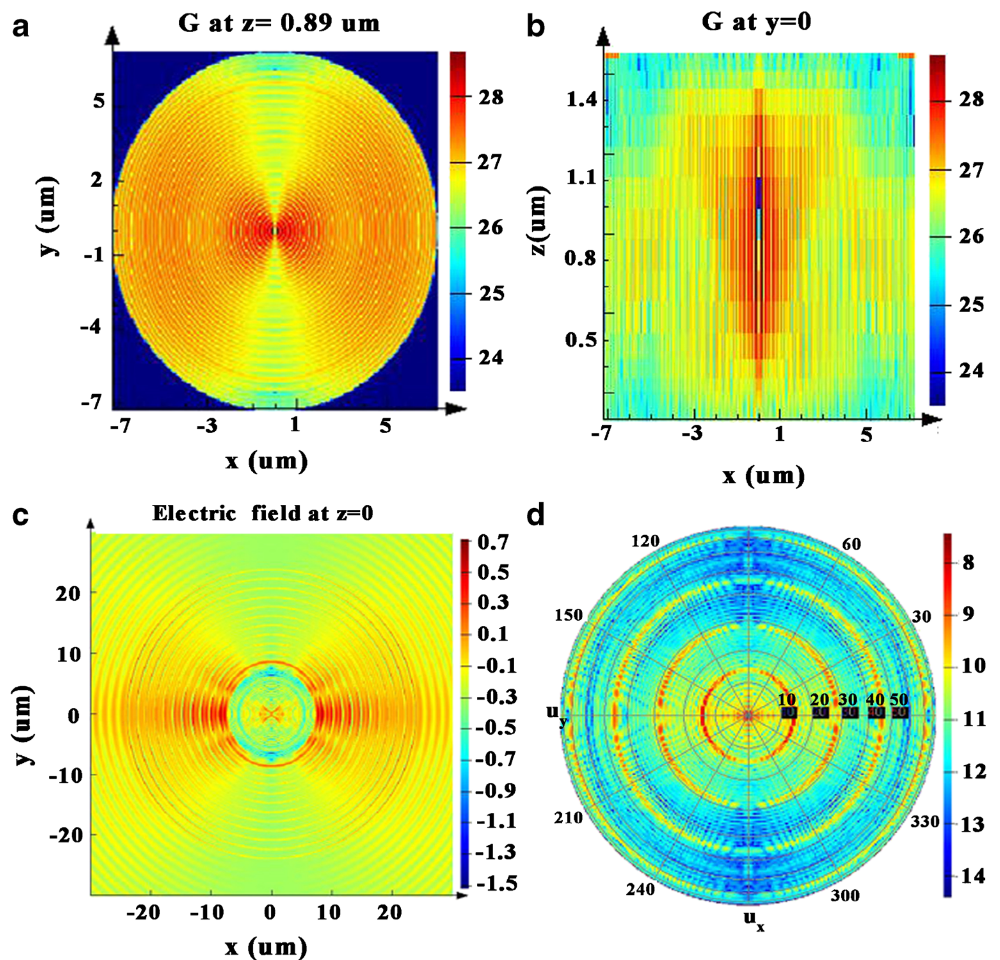

Fig. 7 Generation rate in the **a** xy and **b** xz planes. Spectral profiles of the **c** electric field and far field spectral profiles are shown in (**a**), (**b**), (**c**), and (**d**). All the plots prove that absorption is very high in the core

Destructive or constructive interference, which is equal to odd or even multiples of π, respectively, occurs depending on the value of φ. The device in constructive interference would behave as an efficient source for unidirectional SPPs that are traveling toward the core region. Figure 5a shows the variation in *Jsc* versus the separation distance between the slit and first groove. A periodic behavior is observed with periodicity that corresponds with the SPP wavelength. The first and second peaks are located at 1220 and 2740 nm, respectively, which corresponds to even values of m in Eq. (4). However, the peaks corresponding to higher modes have lower *Jsc* values, which are attributed to the SPPs loss effect. Consequently, separation distance of 1220 nm is favorable.

Consequently, the constructive interference between SPPs traveling toward the core region and the electromagnetic waves of radiation propagating inside the core region should occur. Thus, Eq. (3) should be applied again to obtain the proper distance. The distance between slit-groove and slit-core regions is predicted to be approximately equal. The first peak at 1120 nm, which differs slightly from the distance between the slit and groove, may be attributed to the partial reflection of SPPs in the core region. Figure 5b shows the variation in *Jsc* with the separation of the slit and core region. The higher modes are excited in this case, but higher modes have lower *Jsc* values. We consider the first modes in our geometry in both cases.

The number of grooves is another important parameter that affects the photocurrent. The photocurrent enhances with the groove numbers for the selected slit-core and slit-groove interspace distances. However, the enhancement rate decreases for cases with more than ten grooves (Fig. 6). Thus, ten grooves is a good tradeoff between size and photocurrent.

The 3D generation rate spectral profile for the optimized parameters is shown in Fig. 7. The xy plot at a desired z-point is shown in Fig. 7a, whereas the zx view at the origin of the core (y = 0) is shown in Fig. 7b. Both plots show that the generation rate is localized within the core because of SPPs confinement. The electric field pattern is shown in Fig. 7c, which represents the slit and grooves that function as the SPPs launcher and focus the SPPs to the core. The far field spectral of the structure is shown in Fig. 7d. The center has the highest energy.

Finally, we obtain the I–V plot of the structure (Fig. 8). The black figure shows the dark current, the red line is the photocurrent of our structure, and the purple curve is for the bare Si-Ge photodetector. The result shows that the photocurrent is enhanced by 13-fold compared with bare Si-Ge photodetector. Moreover, the SPPs only modify the photocurrent and do not affect the breakdown voltage (the corresponding voltage for the current of 10 μA) and punch-through voltage. The punch-through and breakdown voltages are 3 and 27.7 V, respectively.

Summary

SPPs can be utilized in conventional photodetectors to enhance photodetection and downscale the dimensions of a photodetector. Moreover, the proposed structure is very attractive for industrial purposes, because it is Si-based, and compatible with the CMOS process. Photodetection is remarkably enhanced by 13-fold. We also present the variation in the photocurrent with geometrical parameters. Employing SPPs in semiconductor can boost their functionality, and our structure can be utilized in different photodetector configurations.

Acknowledgments This work was supported partially by the National Natural Science Foundation of China (Grant nos. 61675195), the funding of the Chinese Academy of Sciences President's International Fellowship Initiative (2014FFGB0023), the China Postdoctoral Science Foundation (2015M581150), the Natural Science Foundation of Beijing Municipality (2142031), the Beijing Municipal Science and Technology Commission project (Z141100003814002 and Z151100003315019), the Major State Basic Research Development Program of China (2013CB632103), the Scientific Research Foundation for the Returned Overseas Chinese Scholars, State Education Ministry and the Chinese Academy of Sciences and the bilateral collaboration project between Chinese Academy of Sciences and Japan Society for the Promotion of Science (GJHZ1316). The authors are grateful to Dr. Ahsan Alam for technical support from Lumerical Company and Mrs. Moradi for her assistance during the preparation of the manuscript.

References

1. Alexander SB (1997) Optical communication receiver design. SPIE Optical engineering press Bellingham, Washington
2. Kyomasu M (1995) Development of an integrated high speed silicon PIN photodiode sensor. IEEE Trans. Electron Dev. 42:1093–1099
3. Zimmermann H, Müller B, Hammer A, Herzog K, Seegebrecht P (2002) Large-area lateral pin photodiode on SOI. IEEE Trans. Electron Dev. 49:334–336
4. Yao Y, Liu X, Li Y, Zhang Z, Ren T (2015) A novel PIN photodetector with double linear arrays for rainfall prediction. J Semicond 36:094011
5. Colace L, Masini G, Galluzzi F, Assanto G, Capellini G, Di Gaspare L, Palange E, Evangelisti F (1998) Metal–semiconductor–metal

near-infrared light detector based on epitaxial Ge/Si. Appl Phys Lett 72:3175–3177

6. Kong X, Liu C, Dong W, Zhang X, Tao C, Shen L, Zhou J, Fei Y, Ruan S (2009) Metal-semiconductor-metal TiO_2 ultraviolet detectors with Ni electrodes. Appl Phys Lett 94:123502
7. C. Xue, H. Xue, B. Cheng, A. Bai, W. Hu, Y. Yu, and Q. Wang, Si/Ge separated absorption charge multiplication avalanche photodetector with low dark current, in *Proceedings of IEEE International Conference on Group IV Photonics (IEEE, 2009)*, pp. 178–180
8. Michel J, Liu J, Kimerling LC (2010) High-performance Ge-on-Si photodetectors. Nature Photon 4:527–534
9. Li B, Yang X, Yin W, Lu Q, Cui R, Han Q (2014) A high-speed avalanche photodiode. J Semicond 35:074009
10. Gity F, Hayes JM, Corbett B, Morrison AP (2011) Modeling the effects of interface traps on the static and dynamic characteristics of Ge/Si avalanche photodiodes. IEEE J Quantum Electron 47: 849–857
11. Zaoui WS, Chen H-W, Bowers JE, Kang Y, Morse M, Paniccia MJ, Pauchard A, Campbell JC (2009) Frequency response and bandwidth enhancement in Ge/Si avalanche photodiodes with over 840 GHz gain-bandwidth-product. Opt Express 17(15): 12641–12649
12. M. Huang, P. Cai, L. Wang, T. Shi, W. Chen, S. Li, G. Hou, C.-y. Hong, and D. Pan 2014, Development of Si photonics technology: Ge/Si avalanche photodiode for PON applications, in *Optical Fiber Communication Conference*, (Optical Society of America, 2014), paper Tu2C. 2
13. Kang Y, Mages P, Clawson A, Yu P, Bitter M, Pan Z, Pauchard A, Hummel S, Lo Y (2002) Fused InGaAs-Si avalanche photodiodes with low-noise performances. IEEE Photon Technol Lett 14: 1593–1595
14. S. Radic, D. Moss, and B. Eggleton, Optical Fiber Telecommunications VA: Components and Subsystems, (Academic Press, 2008), Chap. 20
15. Assefa S, Xia F, Vlasov YA (2010) Reinventing germanium avalanche photodetector for nanophotonic on-chip optical interconnects. Nature 464:80–84
16. D. Dai, H.-W. Chen, J. E. Bowers, Y. Kang, M. Morse, and M. J. Paniccia, Equivalent circuit model of a Ge/Si avalanche photodiode, in *Proceedings of IEEE Conference on Group IV Photonics* (IEEE, 2009), pp. 9–11
17. A. V. Zayats and S. Maier, Active plasmonics and tuneable plasmonic metamaterials (John Wiley & Sons, 2013)
18. Barnes WL, Dereux A, Ebbesen TW (2003) Surface plasmon subwavelength optics. Nature 424:824–830
19. Chalabi H, Schoen D, Brongersma ML (2014) Hot-electron photodetection with a plasmonic nanostripe antenna. Nano Lett 14:1374–1380
20. Sobhani A, Knight MW, Wang Y, Zheng B, King NS, Brown LV, Fang Z, Nordlander P, Halas NJ (2013) Narrowband photodetection in the near-infrared with a plasmon-induced hot electron device. Nature Commun 4:1643
21. Ditlbacher H, Aussenegg F, Krenn J, Lamprecht B, Jakopic G, Leising G (2006) Organic diodes as monolithically integrated surface plasmon polariton detectors. Appl Phys Lett 89:1101
22. Li L, Yu Y (2014) Surface-plasmon-enhanced light transmission intensity with a basic grating in GaN-based LED. J Semicond 35: 043003
23. Bavil MA, Zhou Z, Deng Q (2013) Active unidirectional propagation of surface plasmons at subwavelength slits. Opt Express 21: 17066–17076
24. Bavil MA, Deng Q, Zhou Z (2014) Extraordinary transmission through gain-assisted silicon-based nanohole arrays in telecommunication regimes. Opt Lett 39:4506–4509
25. Ebbesen TW, Lezec HJ, Ghaemi H, Thio T, Wolff P (1998) Extraordinary optical transmission through sub-wavelength hole arrays. Nature 391:667–669
26. López-Tejeira F, Rodrigo SG, Martín-Moreno L, García-Vidal FJ, Devaux E, Ebbesen TW, Krenn JR, Radko I, Bozhevolnyi SI, González MU (2007) Efficient unidirectional nanoslit couplers for surface plasmons. Nature Phys 3:324–328
27. Liu Y, Palomba S, Park Y, Zentgraf T, Yin X, Zhang X (2012) Compact magnetic antennas for directional excitation of surface plasmons. Nano Lett 12:4853–4858
28. Lin J, Mueller JB, Wang Q, Yuan G, Antoniou N, Yuan X-C, Capasso F (2013) Polarization-controlled tunable directional coupling of surface plasmon polaritons. Science 340:331–334
29. Kumar P, Tripathi V, Kumar A, Shao X (2015) Launching focused surface plasmon in circular metallic grating. J Appl Phys 117: 013103
30. Warburton RE, Intermite G, Myronov M, Allred P, Leadley DR, Gallacher K, Paul DJ, Pilgrim NJ, Lever LJ, Ikonic Z (2013) Ge-on-Si single-photon avalanche diode detectors: design, modeling, fabrication, and characterization at wavelengths 1310 and 1550 nm. IEEE Trans. Electron Dev. 60:3807–3813
31. Herbert D (1998) Theory of SiGe waveguide avalanche detectors operating at $\lambda = 1.3\ \mu m$. IEEE Trans Electron Dev 45:791–796
32. Johnson PB, Christy R-W (1972) Optical constants of the noble metals. Phys Rev B 6:4370
33. Marburger J, Felber F (1978) Theory of a lossless nonlinear Fabry-Perot interferometer. Phys Rev A 17:335